An Open Rectangular Waveguide Grating for Millimeter-Wave Traveling-Wave Tubes *

Ming-Liang Liao(廖明亮)[1,2], Yan-Yu Wei(魏彦玉)[1**], Hai-Long Wang(王海龙)[1,2], Yu Huang(黄宇)[4], Jin Xu(徐进)[1], Yang Liu(刘漾)[1,2], Guo Guo(郭骥)[1], Xin-Jian Niu(牛新建)[1], Yu-Bin Gong(宫玉彬)[1], Gun-Sik Park[3]

[1]*National Key Laboratory of High Power Vacuum Electronics, School of Physical Electronics, University of Electronic Science and Technology of China, Chengdu 610054*

[2]*Southwest China Research Institute of Electronic Equipment (CETC 29), Chengdu 610036*

[3]*Center for THz-Bio Application Systems, Department of Physics and Astronomy, Seoul National University, Seoul 151-747, Korea*

[4]*Engneering and Technical College, Chendu University of Technology, Leshan 614007*

(Received 6 April 2016)

Millimeter-wave traveling-wave tube (TWT) prevails nowadays as the amplifier for radar, communication and electronic countermeasures. The rectangular waveguide grating is a promising all-metal interaction circuit for the millimeter-wave TWT with advantages of high power capacity, fine heat dissipation, scalability to smaller dimensions for shorter wavelengths, compact structure and robust performance. Compared with the traditional closed structure, the open rectangular waveguide grating (ORWG) has wider bandwidth, lower cut-off frequency, and higher machining precision for higher working frequencies due to the open transverse. It is a potential structure that can work in the millimeter wave and even Terahertz band. The rf characteristics including dispersion and interaction impedance are investigated by both theoretic calculation and software simulation. The influences of the structure parameters are also discussed and compared, and the theoretical results agree well with the simulation results. Based on the study, the ORWG will favor the design of a broadband and high-power millimeter-wave TWT.

PACS: 07.57.Hm, 42.60.Da, 41.20.Jb DOI: 10.1088/0256-307X/33/9/090701

Traveling wave tubes (TWTs) have significant applications in communication, electronic countermeasures, radar, and remote sensing as millimeter-wave amplifiers with advantages of stability, reliability, high power and broad bandwidth.[1−3] In recent years, demand of high-frequency and high-power TWT for advanced radar and communication has been emerging, which works between 40 and 300 GHz with peak power up to several hundreds of kilowatts, together with bandwidth up to 10%. As the core part where the electron beam and electromagnetic (EM) wave interact for energy transmission, the slow-wave structure (SWS) determines the performance of a TWT.[4] Among the typical SWS, the helix has a broad bandwidth and limited power capacity, while the coupled cavity supports high power in narrow bandwidth. The helix is widely used in communication and electronic countermeasures which ask for broad band, and coupled cavity prevails in radar for the large pulse power.[5] After investigation of interaction mechanisms among the different SWSs, rectangular waveguide grating (RWG) has advantages over the helix and coupled cavity for the simple structure, low-cost and precise machining, high power capacity, robust performance, fine heat dissipation and the scalability to shorter wavelengths. Therefore, RWG has been widely studied in the past years. For example, McVey *et al.*[6] and Booske *et al.*[7] adopted the widespread method called single mode approximation to carry out many theoretical research studies and experiments. Zaginaylov *et al.* proposed a singular integral equation method to accurately investigate dispersion properties and field distributions inside an RWG used in low-voltage TWT.[8,9] Maragos *et al.* presented an eigenmode approach which gives the dispersion relation directly and very fast.[10] Lu *et al.* analyzed the RWG with arbitrary shaped grooves to find a type of better dispersion.[11]

The investigation on RWG shows that this structure is intensively dispersive, which restricts the broadband application. Therefore, the metamorphosis with an open transverse comes to our minds. As an open all-metal circuit, the open rectangular waveguide grating (ORWG) shown in Fig. 1 not only has much wider bandwidth than the closed structure, but also supports higher machining precision for higher working frequencies due to the open transverse, which can

*Supported by the National Natural Science Foundation of China under Grant No 61271029, the National Science Fund for Distinguished Young Scholars of China under Grant No 61125103, and the National Research Foundation of Korea under Grant No MSIP: NRF-2009-0083512.

**Corresponding author. Email: yywei@uestc.edu.cn

© 2016 Chinese Physical Society and IOP Publishing Ltd

be used as interaction circuits for Orotron, backward wave tube, relativistic TWT, and advanced schemes of gyrotrons, etc.[12–17]

The geometrical parameters are labeled in Fig. 2. The axial period is L, the groove's depth and width are p and s, respectively, b is the height of the waveguide, and the transverse width of the structure is a. Expressed in terms of rectangular coordinates x, y, z, the space of the ORWG SWS can be divided into two parts: interaction region I and groove region Ⅱ.

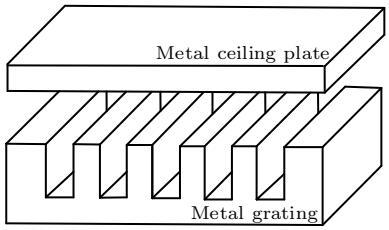

Fig. 1. The 3D picture of the open rectangular grating waveguide.

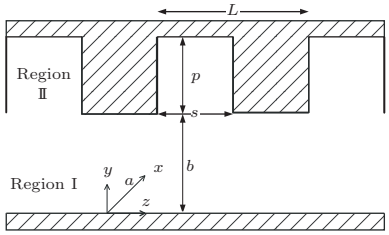

Fig. 2. The 2D illustrative picture.

As an open structure, ORWG supports TE or TM mode. Since a strong axial electric field is needed to interact with the electron beam, we consider only TM mode here. In this mode, we can calculate H_x firstly, and then the other components of electromagnetic (EM) field can be expressed through H_x. Since the transverse is open, we assume that the waveguide width is infinite and ignore the edge effects. In this way, the field components can be approximately seen as not changed versus the transverse direction x, helping us to obtain a fast and simple result. In the following analysis, a time $\exp(j\omega t)$ dependence is assumed (and suppressed) for all field quantities. Using Floquet's theorem, the field components in the interaction region I can be obtained as

$$H_x = \sum_{n=-\infty}^{\infty} a_n \cosh(\gamma_n y) e^{-j\beta_n z}, \tag{1}$$

$$\begin{aligned} E_y &= -j\frac{\omega\mu_0}{k_0^2}\frac{\partial H_x}{\partial z} \\ &= -\frac{\omega\mu_0}{k_0^2}\sum_{n=-\infty}^{\infty} a_n\beta_n \cosh(\gamma_n y) e^{-j\beta_n z}, \end{aligned} \tag{2}$$

$$\begin{aligned} E_z &= j\frac{\omega\mu_0}{k_0^2}\frac{\partial H_x}{\partial y} \\ &= j\frac{\omega\mu_0}{k_0^2}\sum_{n=-\infty}^{\infty} a_n\gamma_n \sinh(\gamma_n y) e^{-j\beta_n z}, \end{aligned} \tag{3}$$

$$E_x = H_y = H_z = 0, \tag{4}$$

where a_n is the amplitude factor, and $\beta_n = \beta_0 + (2\pi n/L)$ is the axial propagation constant of the nth space harmonic, $\gamma_n = \sqrt{\beta_n^2 - k_0^2}$ is the radial propagation constant, k_0 is the free-space wave number, and n, ω and μ_0 are the order of the space harmonics, angular frequency, and permeability of free space, respectively.

The field components in the groove region Ⅱ can be obtained as

$$H_x = \sum_{m=0}^{\infty} b_m \cosh[l_m(h-y)] \cos\left(\frac{m\pi z}{s}\right), \tag{5}$$

$$\begin{aligned} E_y &= -j\frac{\omega\mu_0}{k_0^2}\frac{\partial H_x}{\partial z} \\ &= j\frac{\omega\mu_0}{k_0^2}\frac{\pi}{s}\sum_{m=0}^{\infty} m b_m \cosh[l_m(h-y)] \sin\left(\frac{m\pi z}{s}\right), \end{aligned} \tag{6}$$

$$E_z = j\frac{\omega\mu_0}{k_0^2}\sum_{m=0}^{\infty} b_m l_m \sinh[l_m(h-y)] \cos\left(\frac{m\pi z}{s}\right), \tag{7}$$

where b_m is the amplitude factor, $l_m^2 = (\frac{m\pi}{s})^2 - k_0^2$, $h = b + p$, and m is the order of the space harmonic.

To obtain the dispersion equation, the following matching conditions of fields are needed on surface $y = b$,

$$\begin{aligned} &H_x^{\mathrm{I}} = H_x^{\mathrm{II}}, \quad 0 < z < s, \Big|_{y=b} \\ &E_z^{\mathrm{I}} = \begin{cases} E_z^{\mathrm{II}}, & 0 < z < s, \\ 0, & s < z < l, \end{cases} \Big|_{y=b}. \end{aligned} \tag{8}$$

That is,

$$\begin{aligned} &\sum_{n=-\infty}^{\infty} a_n \cosh(\gamma_n b) e^{-j\beta_n z} \\ &= \sum_{m=0}^{\infty} b_m \cosh[l_m(h-b)] \cos\left(\frac{m\pi z}{s}\right), \quad 0 \le z \le s, \end{aligned} \tag{9}$$

$$\begin{aligned} &\sum_{n=-\infty}^{\infty} a_n\gamma_n \sinh(\gamma_n b) e^{-j\beta_n z} \\ &= \begin{cases} \sum\limits_{m=0}^{\infty} b_m l_m \sinh[l_m(h-b)] \cos(\frac{m\pi z}{s}), & 0 \le z \le s, \\ 0, & s \le z \le L. \end{cases} \end{aligned} \tag{10}$$

With the above matching conditions and employing the orthogonal properties of trigonometric functions,

the dispersion equation can be derived as

$$\frac{1}{\tan(k_0 p)} = \frac{s}{L}\sum_{n=-\infty}^{\infty}\left[\frac{\sin(\beta_n s/2)}{\beta_n s/2}\right]^2 \frac{k_0}{\gamma_n \tanh(\gamma_n b)}. \quad (11)$$

From Pierce's theory, the interaction impedance of the mth space harmonic is written as

$$Kc(m) = \frac{E_{zm}E_{zm}^*}{2\beta_m^2 P}, \quad (12)$$

where E_{zm} is the longitudinal electric-field component of the mth space harmonic, E_{zm}^* is the conjugate, β_m is the axial propagation constant of the mth space harmonic, and P is the total power flowing through the circuit.

For the standing wave existing in the groove region, P equals the power flow in region I. We choose E_{zm} at $y = b$ to calculate due to the fact that the electric field is strongest around here. Employing Eqs. (1) and (2), we can obtain the expression of total power using the integration of Poynting vector

$$\begin{aligned} P = P_{\rm I} &= \sum_{n=-\infty}^{\infty}\frac{1}{2}{\rm Re}\iint -E_{yn}\cdot H_{xn}^* ds \\ &= \sum_{n=-\infty}^{\infty}\frac{1}{2}a\frac{\omega\mu_0}{k_0^2}|a_n|^2\beta_n\left(\frac{b}{2}+\frac{\sinh(2\gamma_n b)}{4\gamma_n}\right), \end{aligned} \quad (13)$$

where

$$\gamma_n = \sqrt{\beta_n^2 - k_0^2},$$
$$a_n = sAe^{\frac{j\beta_n s}{2}}\frac{1}{\gamma_n \sinh(\gamma_n b)}\cdot{\rm sinc}\left(\frac{\beta_n s}{2}\right),$$

with A being a constant, and ${\rm sinc}(x) = \frac{\sin x}{x}$.

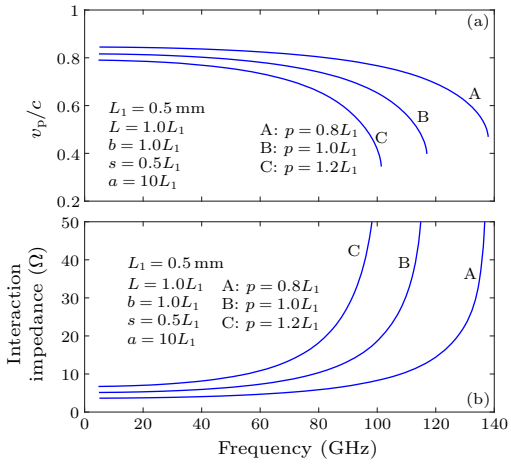

Fig. 3. (a) Dispersion versus groove's depth. (b) Interaction impedance versus groove's depth. Hereafter $V_{\rm P}$ represents the phase velocity, and c represents the velocity of light in a vacuum.

Substituting Eqs. (3) and (13) into Eq. (12), we can obtain the expression of the interaction impedance

$$\begin{aligned} Kc(m) = &\left[\frac{\omega\mu_0}{k_0^2}\left({\rm sinc}\left(\frac{\beta_m s}{2}\right)\right)^2\right] \\ &\cdot\left[a\beta_m^2\sum_{n=-\infty}^{\infty}\left(\frac{b}{2}+\frac{\sinh(2\gamma_n b)}{4\gamma_n}\right)\cdot\left({\rm sinc}\left(\frac{\beta_n s}{2}\right)\right)^2\right. \\ &\left.\cdot\left(\frac{1}{\gamma_n\sinh(\gamma_n b)}\right)^2\beta_n\right]^{-1}. \end{aligned} \quad (14)$$

To obtain a more effective beam–wave coupling, larger interaction impedance and better synchronous velocity between the EM wave and the electron beam are needed in an SWS. Large interaction impedance supports higher interaction efficiency and small dispersion sustains the synchronous condition in a broader band. Based on the equations of dispersion and interaction impedance, we wrote a program with MATLAB to analyze the influences of physical dimensions on the rf properties.

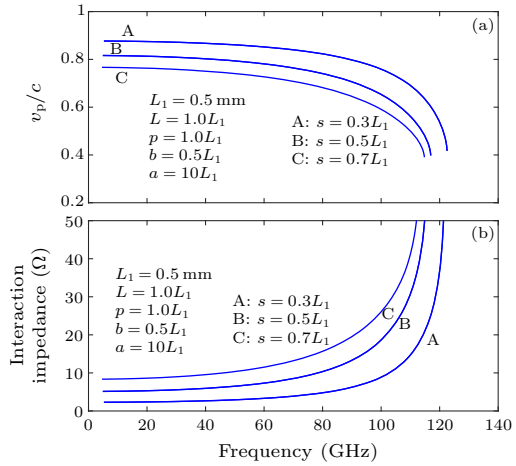

Fig. 4. (a) Dispersion versus groove's width. (b) Interaction impedance versus groove's width.

Figures 3 and 4 show the influences of groove's size on rf properties. With increasing the groove's depth or width, the higher cut-off frequency moves down, the dispersion property becomes worse while the interaction impedance becomes better. Therefore, larger groove will promote the interaction efficiency but will sacrifice some bandwidth.

Figures 5 and 6 show the influences of groove's period and the height of the waveguide on rf properties, respectively. With increasing these dimensions, the dispersion property becomes barely better in the majority of the possible working band while the interaction impedance becomes notably smaller. Therefore, shorter groove's period and shorter height of the waveguide will maintain the bandwidth while providing higher interaction efficiency.

Figure 7 shows that shorter waveguide's width will lead to larger interaction impedance. Because the ORWG is an open structure and the dispersion prop-

erty is not influenced by the width according to dispersion Eq. (11), we just compare the effects on interaction impedance.

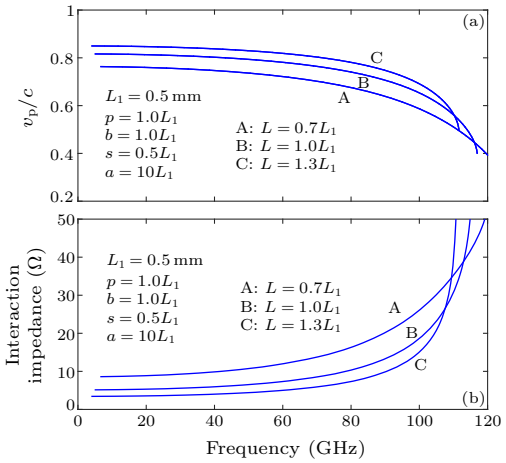

Fig. 5. (a) Dispersion versus groove's period. (b) Interaction impedance versus groove's period.

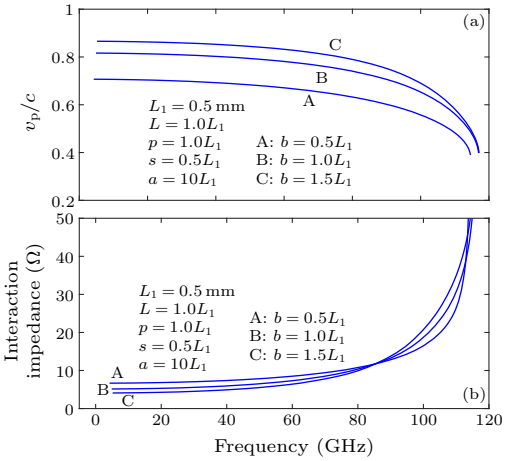

Fig. 6. (a) Dispersion versus the height of the waveguide. (b) Interaction impedance versus the height of the waveguide.

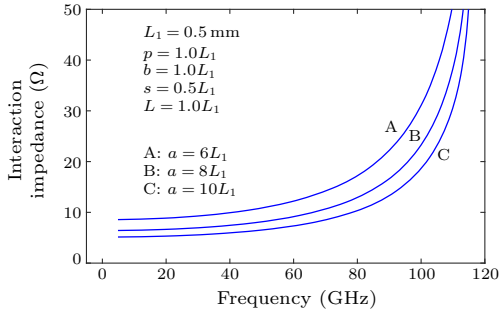

Fig. 7. Interaction impedance versus waveguide's width.

The theoretical study of the parameter variation shows that larger size of groove will benefit the interaction efficiency but will sacrifice some bandwidth, while shorter groove's period, shorter height and width of the waveguide will bring higher interaction efficiency and maintain the bandwidth.

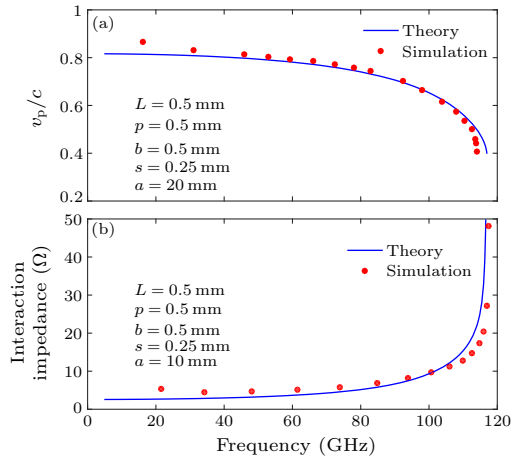

Fig. 8. (a) Comparison of (a) dispersion and (b) interaction impedance between theory and simulation.

A 3D electromagnetic code HFSS is adopted to simulate the rf properties in comparison with the theoretical results. Figure 8 indicates that the simulation matches well with the theory. The inconformity near the lower cut-off frequency is due to the waveguide's open width which is assumed to be infinite in theory but finite in real simulation model. If we choose a longer waveguide's width to make the comparison, especially for the dispersion equation not influenced by this parameter in our simplified algorithm, the theory and simulation will match even better.

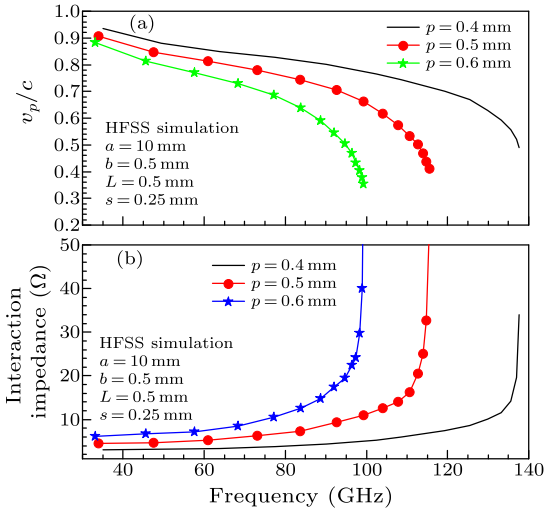

Fig. 9. Simulation of (a) dispersion and (b) interaction impedance versus groove's depth.

Figures 9 and 10 are the simulations on parameter changes. As a representative example, we present the typical parameters of groove's depth and period here to verify the theory. Similar to the theoretical results, longer groove's depth is good for interaction impedance and bad for dispersion, while shorter groove's period benefits the interaction impedance and barely influences dispersion. Simulations on the other

parameters also have good agreements with theory, which are not presented due to the space limitation.

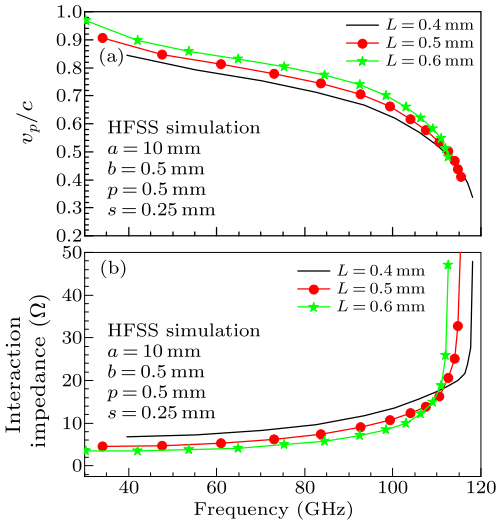

Fig. 10. Simulation of (a) dispersion and (b) interaction impedance versus groove's period.

In summary, an ORWG has been presented, which can support much wider bandwidth than the traditional closed structure. The rf characteristics including dispersion and interaction impedance are investigated by both theoretical calculation and software simulation. The influences of structure parameters are also discussed and compared, and the theoretical results agree well with the simulation results. As an all-metal circuit with simple structure, the ORWG will favor the design of a broadband and high-power TWT that can work in the millimeter wave and even Terahertz band.

References

[1] He J et al 2009 *Chin. Phys. Lett.* **26** 114103
[2] Liao M L et al 2009 *Chin. Phys. Lett.* **26** 114207
[3] Wei Y Y et al 2014 *IEEE Electron Device Lett.* **35** 1058
[4] Wang W X et al 2003 *Int. J. Infrared Millimeter Waves* **24** 1469
[5] Liao M L et al 2010 *IEEE Trans. Plasma Sci.* **38** 1574
[6] McVey B D et al 1994 *IEEE Trans. Microwave Theory Tech.* **42** 995
[7] Joe J et al 1994 *Phys. Plasmas* **1** 176
[8] Zaginaylov G I et al 2000 *IEEE Trans. Plasma Sci.* **28** 614
[9] Zaginaylov G I et al 2002 *IEEE Trans. Plasma Sci.* **30** 1151
[10] Maragos A A et al 2003 *IEEE Trans. Plasma Sci.* **31** 1075
[11] Lu Z G et al 2007 *Int. J. Infrared Millimeter Waves* **27** 791
[12] Collin R E 1966 *Foundation of Microwave Engineering* (New York: Mc-Graw-Hill)
[13] Huang Y 2007 *Master Dissertation* (Chengdu: University of Electronic Science and Technology of China)
[14] Marshall E M et al 1988 *IEEE Trans. Plasma Sci.* **16** 199
[15] Leavitt R P et al 1979 *Appl. Phys. Lett.* **35** 363
[16] Vavriv D M and Schuenemann K 1998 *Phys. Rev.* E **57** 5993
[17] Leou K C et al 1998 *IEEE Trans. Plasma Sci.* **26** 518